

## Trend analysis development of urban heat island using thermal remote sensing

Mahsa Bozorgi<sup>1\*</sup>, Nejadkoorki Farhad<sup>1</sup>, Bihamta Toosi Neda<sup>2</sup>

<sup>1</sup> Department of Environmental Science, Yazd University, Yazd, Iran

<sup>2</sup> Department of Natural Resources, Isfahan University of Technology, Isfahan

### Article history:

Received: 10 March 2020, Received in revised form: 15 August 2020, Accepted: 20 August 2020

### ABSTRACT

Population growth and urbanization development are the major factors in increasing land surface temperature (LST) in urban areas which lead to Urban Heat Island (UHI). Green covers play an important role in improving the comfort level of citizens and achieving a sustainable urban environment through decreasing temperature, increasing humidity, and finally dwindling UHI. The current study aims to analyze and evaluate the changes of green covers and LST in Isfahan Metropolitan Area (IMA), Iran, from 1998 to 2014. This study emphasizes the impact of green covers on IMA temperature patterns. Accordingly, Normalized Difference Vegetation Index (NDVI) threshold method was applied to obtain the land surface emissivity (LSE). In addition, Planck's law for TM image and Split Window (SW) algorithm for OLI/TIRS image were utilized in order to retrieve LST. It was validated with data collected from 5 stations within the city. Temporal and spatial changes in IMA's LST were then analyzed using statistical methods, Mann-Kendall analysis, and Urban-Heat-Island Ration Index (URI). The result indicates that LST in IMA had an increasing trend over the study period and its intensity, generally, concentrated in the northwest and the northeast of the city, the bed of dried Zayandeh-Rood and green covers along the river bank which destroyed. Also, there was an increasing trend in URI from 0.25 in 1998 to 0.312 in 2014. All in all, it can be concluded Mann-Kendall trend test and URI were appropriate outfits to analyze satellite images in order to identify the Spatio-temporal change of UHI.

### KEYWORDS

Land surface temperature  
Urban heat island  
Mann-Kendall Analysis  
Normalized Difference Vegetation Index  
Landsat

### 1. Introduction

Urbanization is considered one of the most effective anthropogenic activities in the second half of the 20<sup>th</sup> century (Singh et al., 2017). Urbanization development has led to extensive landscape changes through the transformation of land cover. Such a mechanism is associated with many feedbacks and feedback loops with surrounding ecosystems, which subsequently alter and modify the functioning of the cities and ecosystems (Gobakis et al., 2011; Wu 2014).

Green covers reduction which continuously occurs as a result of urban development, not only affects land surface temperature (LST) in urban areas, (Singh et al., 2017) but also leads to carbon dioxide accumulation in the atmosphere

(Islam & Islam, 2013).

Through urbanization natural land is converted into built-up land which leads to significant changes in urban structures and mechanisms (Jing & Guangjin, 2011). This process is associated with many negative environmental consequences such as soil compaction, sealing, organic matter decline, biodiversity loss, air pollution, water contamination, and the well-known Urban Heat Island (UHI) phenomenon (Oke, 1987; Rosenfeld et al., 1998; Voogt & Oke 2003).

In urban environments, built-up structures have a higher thermal capacity (Taha 1997) and such locations can absorb higher temperatures during the daytime and release more heat fluxes during nighttime. Based on Oke (1995), UHI is

\* Corresponding author

E-mail addresses: mahsabozorgi@stu.yazd.ac.ir (M. Bozorgi); f.nejadkoorki@yazd.ac.ir (F. Nejadkoorki); n.bihamtaitoosi@na.iut.ac.ir (N. Bihamta Toosi)

DOI: 10.22059/eoge.2021.309046.1086

referred to as the difference between urban and non-urban surrounding environments, which is a direct result of land-use conversion and human energy use. These differences are mainly due to land-use change caused by the urbanization process that largely replaces soil and vegetative covers with impervious surfaces. These surface alternations consequently affect albedo, thermal capacity, and heat conductivity over cities, which then modify the thermal environment and micro-climate of the cities (Zhou et al., 2011). Higher temperatures resulted from the UHI phenomenon can in turn lead to increased water consumption, elevated energy use, and the formation of secondary air pollutants such as ground-level ozone, which causes respiratory problems to urban dwellers (Akbari et al., 2001).

Therefore, an improved understanding of UHI variability over temporal and spatial scales can assist urban planners to detect high-risk zones in cities and take appropriate preventive and restorative measures. In addition, monitoring the Spatio-temporal variability of the UHI phenomenon can provide valuable planning implications for planting green covers and landscape design (Asgarian et al., 2015).

Part of information for such purpose can be obtained from thermal remote sensing technology and this topic has also been an active research agenda in the literature, which attracted considerable attention from scholars in different parts of the world.

## 1.2 Literature review

Previous UHI studies have mainly concentrated on the effects of land-use composition and configuration on land surface temperature (LST) and remotely sensed data has been largely employed to evaluate LST patterns and UHI spatial distributions. Amiri et al. (2009) conducted a temporal study to analyze the relationships between different land-use categories and LST patterns. In this regard, the temperature vegetation index (TVX) space was calculated to investigate the temporal variability of thermal data and vegetation cover. According to their results, the temporal profile of cells in the TVX space indicated a major proportion of changes. The main reason is that urbanization was detectable as pixels transformed from the low temperature-dense vegetation to high temperature-sparse vegetation condition in TVX space. In their review paper, Mirzaei & Haghghat (2010) reported that the UHI phenomenon is associated with considerable impacts on the building's energy and outdoor air quality. In addition, a series of important topics such as treatment of radiation, the effect of trees and pond, and boundary conditions to simulate the behavior of UHI was also discussed. In a further attempt, Zhou et al. (2011) analyzed the relationship between LULC patterns and LST with an emphasis on configuration metrics using correlation analyses and multiple linear regressions. They highlighted that composition of LULC categories is of

higher explanatory power for describing LST variations, however, a wise selection of composition and configuration landscape metrics can be effectively used for urban planning and mitigation of UHI effects. Chakraborty et al. (2013) studied the temporal profile of heat flux values related to the urban and industrial areas in Delhi, India. They concluded that there is an increasing trend for heat flux values, and therefore, LST increase related to the anthropogenic and impervious surfaces.

Chen et al. (2014) evaluated the seasonal effect of urban vegetation and water bodies on urban cool islands (UCIs) at the patch level. The results illustrated that spatial arrangement (size, edge, shape, and connectivity) of urban green clusters are of meaningful effects on their adjacent UCIs in four seasons. Asgarian et al. (2015) also conducted a patch-level analysis of the relationships between urban areas and green covers with UHI. They implemented a step-wise generalized additive modeling method to develop a multiple linear regression model, which found to be the potential to approximately explain half of the UHI variations. Afrakhteh et al. (2016) conducted a scenario-based temporal study to analyze the effect of different urban growth strategies on the thermal landscape of Falavarjan Township, Iran. They highlighted that compared to historical trends; the integrated urban-rural planning perspective is associated with an urban landscape in which rural areas have higher opportunities to grow, while the UHI effect is alleviated across the landscape. Similarly, Chen et al. (2017) investigated diurnal LST variations in urban areas through MODIS Aqua satellite images. They reported that diurnal LST shows an increasing trend with an increase in urbanization. In other words, they indicated increasing diurnal LST variation in response to urbanization implies that urbanization is the potential to yield a higher increase in urban heat absorption than in thermal inertia. Guha & Govil (2020) reported that there is a negative relationship between LST and NDVI and this relationship is stronger in previous times. However, an increase in heterogeneous landscape inside the city boundary changes the LST-NDVI relationship. Yang et al. (2020) showed that the cooling effect of irrigation on daytime LST was higher than night-time LST. Furthermore, the results of validation with synoptic station temperature data and dam water levels as empirical evidence showed that daytime and night-time LST estimates by MODIS image have been significant in this urbanizing dryland.

Considering the above-mentioned researches, some general study patterns can be detected. Firstly, the majority of studies in this field adopted a statistic approach such that the UHI spatial variations over a specific node year were analyzed and temporal variations were largely ignored, which can provide improved planning implications. Besides, similar to the statistical analysis of UHI, temporal studies mainly evaluated the relationships between land-use categories and

LST distribution patterns. In other words, the dynamics of such relationships are the main focus of such studies, while the dynamics of the city thermal environment are disregarded. Therefore, analyzing the Spatio-temporal variability of a city's thermal environment can provide an additional level of knowledge regarding locations that are experiencing an increasing trend of LST. Based on such analysis, a city planner can effectively decide on the optimized location of green cover plantations and alleviate the impact of the UHI phenomenon over the city. Such measures can finally result in improved life quality of urban citizens and more efficient use of water and energy .

**1.3 Research objectives**

This study attempts to utilize remote sensing TIR data in order to analyze LST distribution and Spatio-temporal UHI and comparing them with green cover changes and Zayandeh-Rood River in IMA, Iran from 1998 to 2014. Specifically, the main objectives of this research are as follows:

- Temporal LST mapping and integrating LST layers of two different node years (from 1998 to 2014);
- Temporal NDVI mapping and integrating NDVI layers of two different node years
- Detection of potential UHI hotspots area based on dynamics of thermal environment in IMA; and discussing the main planning implications derived from Spatio-temporal analysis of IMA's thermal environment.

**2. Material and method**

**2.1 Study area**

The study area spans over IMA, central Iran. The area of research location is 115,567 ha bounded between 51° 26' 27" and 51° 49' 58" eastern longitude and 32° 40' 49" and 32° 32' 38" northern latitude (Figure 1). The IMA is of arid and semi-arid climatic conditions (Falihatkar et al., 2011) and the average elevation is 1,575 m above sea level. The annual mean, minimum and maximum air temperature of the study area are 17.2, 24.18, and 10.18 °C, respectively (Isfahan Meteorological Organization, 2014). Zayandeh-Rood River crosses the middle of the city and Soffeh Mountain characterizes the main topography of the location in the south.

**2.2 Image selection and pre-processing**

Landsat 5 TM and Landsat 8 OLI images (LIT level) were

acquired in July 1998 and 2014, respectively. The main reason for selecting the study period was that the largest water storage and continuity of droughts in the region have started since 1998 (Rahimi & Mohamadi, 2017; Karimi et al., 2015). These images were selected for the time when the condition of the urban green cover was in the highest growth. Topographic maps were applied for geometric correction.

Radiances for TIR band of Landsat 5 TM were obtained using Equation 1. Radiance values for Landsat 8 TIRs could be retrieved from Equation 2 (USGS).

$$L_{\lambda} = \left( \frac{LMAX_{\lambda} - LMIN_{\lambda}}{Qcal_{max} - Qcal_{min}} \right) (Qcal_{max} - Qcal_{min}) + LMIN_{\lambda} \quad (1)$$

where  $L_{\lambda}$  is Top of Atmosphere (TOA) spectral radiance (Watts/(m<sup>2</sup>·srad·µm)),  $Qcal$  is the quantized calibrated pixel value in DN,  $LMIN_{\lambda}$  (Watts/(m<sup>2</sup>·srad·µm)) is the spectral radiance scaled to  $Qcal_{min}$ ,  $LMAX_{\lambda}$  (Watts/(m<sup>2</sup>·srad·µm)) is the spectral radiance scaled to  $Qcal_{max}$ ,  $Qcal_{min}$  and  $Qcal_{max}$  are the minimum and maximum quantized calibrated pixel values in DN, respectively (USGS).

Radiance values for Landsat 8 TIRs were retrieved from Equation 2 (USGS).

$$L_{\lambda} = ML \times Qcal + AL \quad (2)$$

where  $L_{\lambda}$  is the TOA spectral radiance (Watts/(m<sup>2</sup>·srad·µm)),  $ML$  is the band-specific multiplicative rescaling factor from the metadata,  $AL$  is the band-specific additive rescaling factor from the metadata,  $QCAL$  is the quantized and calibrated standard product pixel values (DN). The values of  $ML$  and  $AL$  were presented in Table 1 (USGS).

The reflectance value for Landsat 5 TM was calculated from radiance by Equation 3.

$$\rho_{\lambda} = \frac{\pi \cdot L_{\lambda} \cdot d^2}{ESUN_{\lambda} \cdot \cos \theta_s} \quad (3)$$

where  $\rho_{\lambda}$  is planetary reflectance,  $L_{\lambda}$  is the TOA spectral radiance (Watts/(m<sup>2</sup>·srad·µm)),  $d$  is Earth-Sun distance in astronomical units,  $ESUN_{\lambda}$  is the mean solar exo-atmospheric spectral irradiances (Watts/(m<sup>2</sup>·µm)) which can be attained from the handbooks of the related mission and  $\theta_s$  is the solar zenith angle in degrees. Both  $\theta_s$  and  $d$  values can be obtained from the metadata file (USGS).

Reflectance value for Landsat 8 OLI was figured from radiance by Equation 4.

$$\rho_{\lambda}' = Mp \times Qcal + Ap \quad (4)$$

where  $QCAL$  is the quantized and calibrated standard product pixel values (DN). Both  $Mp$  and  $Ap$  is obtained from the metadata (USGS).



LST TM data was generated through Equation 6.

$$K_s = \frac{T}{\left(1 + \frac{\lambda T}{\alpha}\right) \ln \epsilon} \quad (6)$$

where  $\lambda$  is the wavelength of radiance,  $\alpha = hc/k$  ( $h$ =Planck's constant;  $c$ =velocity of light) ( $k$ =Boltzmann constant),  $\epsilon$  is emissivity (Amiri et al., 2009; Artis & Carnahan, 1982).

Then, LST was calculated for TIRS data by Split-Window

Algorithm through Equation 7 (Sobrino et al., 2013)

$$T_s = T_i + c_1 (T_i - T_j) + c_2 (T_i - T_j)^2 + c_0 + (c_3 + c_4 W)(1 - \epsilon)(c_5 + c_6 W) \Delta \epsilon \quad (7)$$

where  $T_i$  and  $T_j$  are the at-sensor brightness temperatures at the SW bands  $i$  and  $j$  (in kelvin),  $\epsilon$  is the mean emissivity,  $\epsilon = 0.5(\epsilon_i + \epsilon_j)$ ,  $\Delta \epsilon$  is the emissivity difference,  $\Delta \epsilon = (\epsilon_i - \epsilon_j)$ ,  $W$  is the total atmospheric water vapor content (in grams per square centimeter), and  $c_0$ - $c_6$  are the SW coefficients (Table 3).

Table 3. Split Window Algorithm Coefficients

Coefficient	C <sub>0</sub>	C <sub>1</sub>	C <sub>2</sub>	C <sub>3</sub>	C <sub>4</sub>	C <sub>5</sub>	C <sub>6</sub>
Value	-0.268	1.378	0.183	54.300	-2.238	-129.200	16.400

### 2.3 LST normalization

In order to establish a basis for logical comparison of bi-temporal LST layers, the effects of time difference were removed applying the minimum and maximum temperature method (Equation 8) (Xunqiang et al., 2011):

$$N_i = \frac{T_{s_i} - T_{s_{min}}}{T_{s_{max}} - T_{s_{min}}} \quad (8)$$

where  $N_i$  is the normalized LST image,  $T_{s_i}$  indicates the LST value of a corresponding pixel,  $T_{s_{min}}$  and  $T_{s_{max}}$  are the minimum and the maximum LST values within raster space, respectively.

### 2.4 LST classification scheme

Bi-temporal normalized LST layers were classified using the mean-standard deviation method (Xu & Chen, 2004; Songlin & Tianxin, 2009). Accordingly, the LST layers were categorized into five classes of low-temperature area, secondary low-temperature area, medium temperature area, secondary high-temperature area, and high-temperature area. Numerical details regarding the classification scheme are provided in Table 4.

Table 4. LST classification scheme based on mean standard deviation method (in this table  $T_s$ ,  $\mu$ , and std respectively indicate normalized LST value, mean and standard deviation)

Temperature classification	Category interval
High temperature	$T_s > \mu + \text{std}$
Secondary high temperature	$\mu + 0.5\text{std} < T_s \leq \mu + \text{std}$
Medium temperature	$\mu - 0.5\text{std} \leq T_s \leq \mu + 0.5\text{std}$
Secondary low temperature	$\mu - \text{std} \leq T_s < \mu - 0.5\text{std}$
Low temperature	$T_s < \mu - \text{std}$

### 2.5 Mann Kendall trend test

Mann-Kendall is a non-parametric test, which is employed

to determine the presence and significance of a trend in UHI of IMA. This method also estimates the starting point of a trend and sharp transitions in the thermal environment (Tayanç et al., 1997). The results of Mann Kendall Test are between '1 and -1' (Mann, 1945; Kendal, 1975).

In Mann-Kendall Test, the null hypothesis,  $H_0$ , supposes that there is an independent realization in data and its distribution are identical and the alternative hypothesis  $H_1$  is that data follow a monotonic trend (Kumar et al., 2009). The test statistic  $S$  was given by:

$$S = \sum_{i=2}^n \sum_{j=1}^{i-1} (\text{sign}(x_i - x_j)) \quad (9)$$

Where  $x_i$  and  $x_j$  are the values of sequence  $i, j$ ;  $n$  is the length of the time series and

$$\text{Sign}(x) = \begin{cases} 1, & \text{if } (x_i - x_j) > 0 \\ 0, & \text{if } (x_i - x_j) = 0 \\ -1, & \text{if } (x_i - x_j) < 0 \end{cases} \quad (10)$$

The mean and the variance of statistics  $S$  as follows:

$$E(S) = 0 \quad (11)$$

If  $n > 10$ :

$$\text{Var}(S) = \frac{n(n-1)(2n+5) \sum_{t=1}^m t_i(t_i-1)(2t_i-5)}{15} \quad (12)$$

$n < 10$ : If

$$\text{Var}(S) = \frac{n(n-1)(2n+5)}{15} \quad (13)$$

Where  $T_i$  is the number of data in the tied group and  $m$  is the number of groups of tied ranks. The standardized test statistic  $Z_{mk}$  was calculated by Equation 14:

$$\frac{S-1}{\sqrt{\text{Var}(S)}} \quad \text{If } S > 0$$

$$0 \quad \text{If } S = 0$$

$$\frac{S+1}{\sqrt{\text{Var}(S)}} \quad \text{If } S < 0 \quad (14)$$

Positive values of  $Z_{mk}$  indicate that the data tend to increase, while negative values of MK illustrate a decreasing trend in data.

**2.6 Urban-Heat-Island Ration Index (URI) calculation**

URI (Xu & Chen, 2004) was considered as a measure to analyze temporal dynamics of the thermal environment in IMA during the 1998–2014-time profile. The URI is calculated according to the following equation:

$$URI = \frac{1}{100m} \sum_{i=1}^n w_i p_i \quad (15)$$

where  $m$  is the number of normal LST categories (here is five),  $n$  refers to the number of LST categories that are of values higher than the normal LST category (here the fourth and fifth categories have a higher temperature compared to the third category which is of a normal temperature),  $w_i$  is the

weighted value of LST categories that are higher than normal LST and  $p_i$  is the area percentage of categories that are of higher values than normal LST to the study area.

**2.7 Normalized difference vegetation index (NDVI)**

NDVI is utilized to quantify vegetation greenness also it is a useful tool in identifying vegetation density and evaluating changes in a plant health situation. NDVI is calculated as a ratio between the red (R) and near-infrared (NIR) values. NDVI is calculated according to the following equation (USGS):

$$(NIR - R) / (NIR + R) \quad (16)$$

The flowchart of methodology was presented in Figure 2.

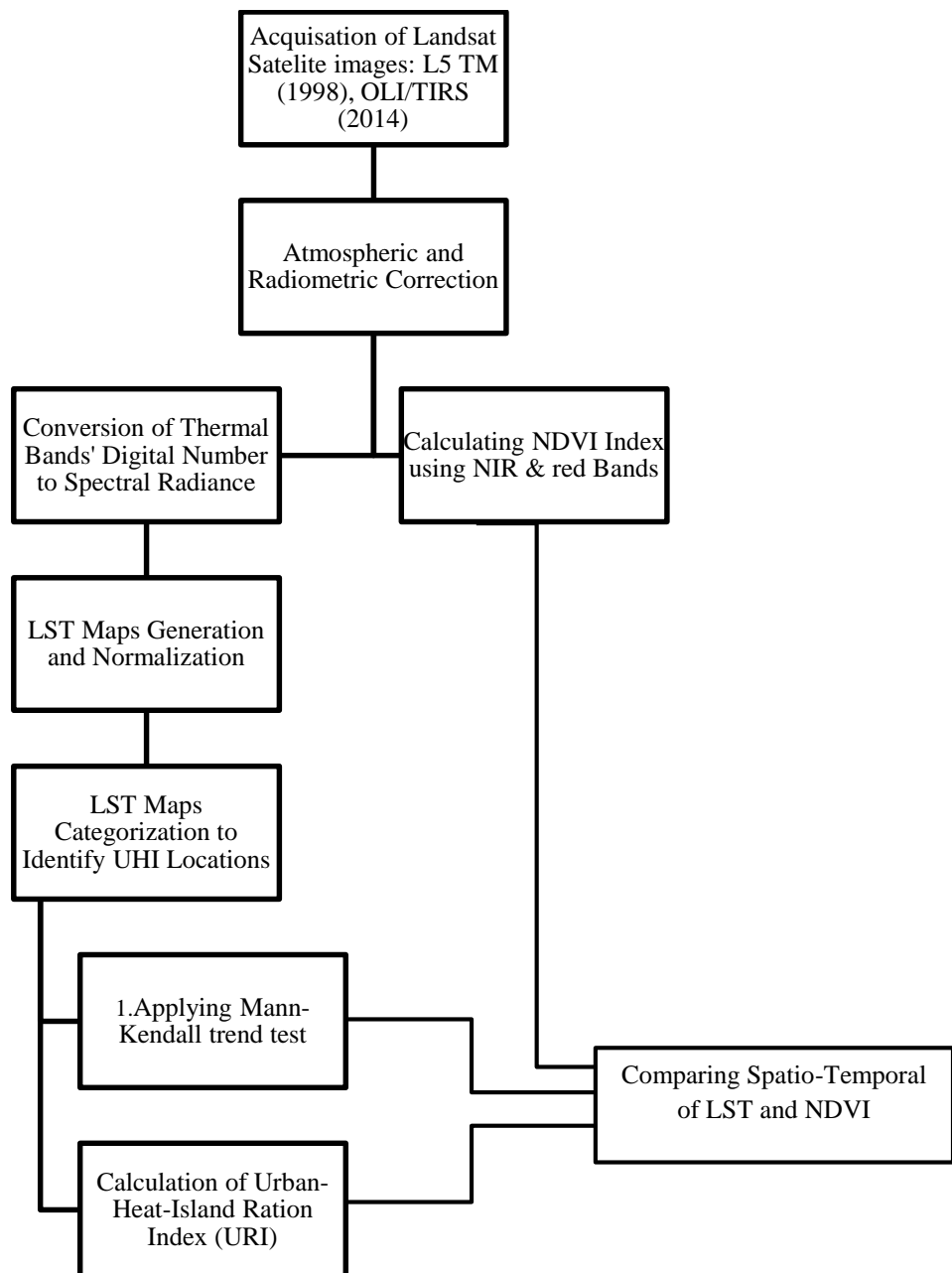


Figure 2. Flowchart of methodology

### 3. Results

NDVI mapping illustrated that major parts of green covers in the vicinity of Zayandeh-Rood River were destroyed over

the study period. Also, green covers in the center, northwest, and northeast of the IMA were converted into industrial and urban areas (Figure 3).

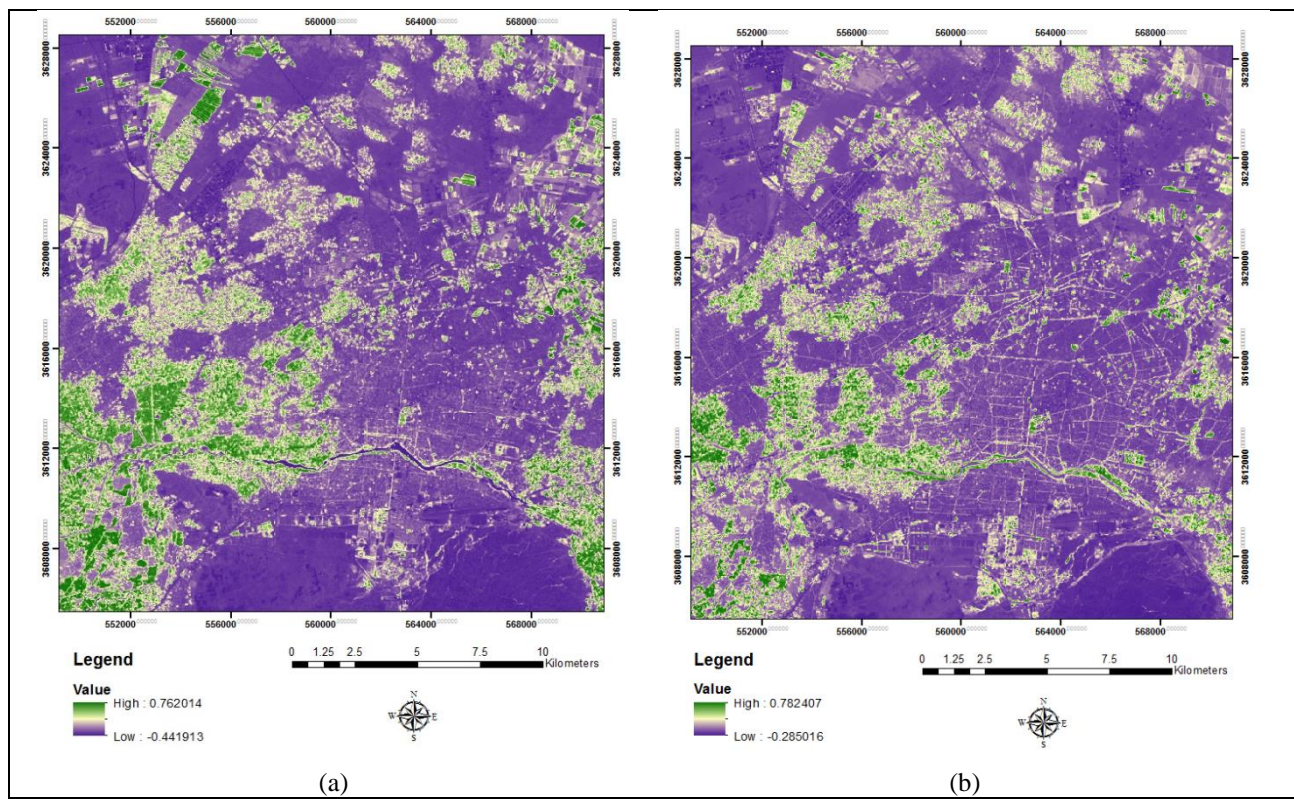


Figure 3. NDVI layers for (a) 1998 and (b) 2014 node years

Bi-temporal LST mapping (Figure 4) indicated the lowest and the highest LST for 1998 were 19 °C and 50 °C, respectively, while these values were correspondingly 28 °C and 57 °C in 2014.

Such a pattern of LST change demonstrates 9 °C increase for the minimum and 7 °C increase for the maximum temperature, which can be considered as a major concern in the region. Statistical parameters derived from LST layers are given in Table 4.

As is illustrated in Figures 3 and 4, the river bank LST has changed significantly during the course. In the image related to 1998, the LST difference among urban versus the river and its green bank area is high. Whereas, the river bank LST is the same as the urban area. Moreover, some spots with high LST have emerged in the dried river bed. Also, some spots with high LST have appeared in the north of the studied area, in 2014. Generally, the highest temperature is observed in the barren land. Bare soil absorbs sunlight and with regard to the low thermal capacity and heat conductivity of soil, its temperature rises quickly. The LST mean in the studied course of time has risen dramatically, from 36.08 °C in the beginning to 43.68 °C in 2014, (Table 5).

#### 3.1 LST classification

For analyzing LST dynamics from 1998 to 2014, normalized LST maps were classified based on the mean-

standard deviation method. Low temperature class was considered as a very cool location and the high temperature class was regarded as the city's hotspot. Consequently, UHI hotspots were detected across the IMA (Figure 5).

As is illustrated in figure 5, the temperature patterns in both images are different. The first category (low) shows the coolest areas. In the image related to 1998, Zayandeh-Rood River and its banks are classified in this category, despite the fact that in the image related to 2014, urban areas are classified as the coolest areas. In hot and arid regions, like the studied area, the suburb is covered with barren lands, and for the same reason, the suburbs have higher LST in regard to the urban areas.

Table 6 shows the areal change of each LST class in the study area during the 1998-2014 timespan. Areas of category five LST are considered as UHI due to their high temperature.

The fifth category (high) shows UHI, and in both images, UHI has expanded in barren lands and salty areas in the suburban part. The results of Table 6 demonstrate that the area of the high-temperature class increased approximately 7% and the area of the medium temperature class decreased by 16%. Furthermore, areas of low temperature and secondary low temperature classes have been unexpectedly increased

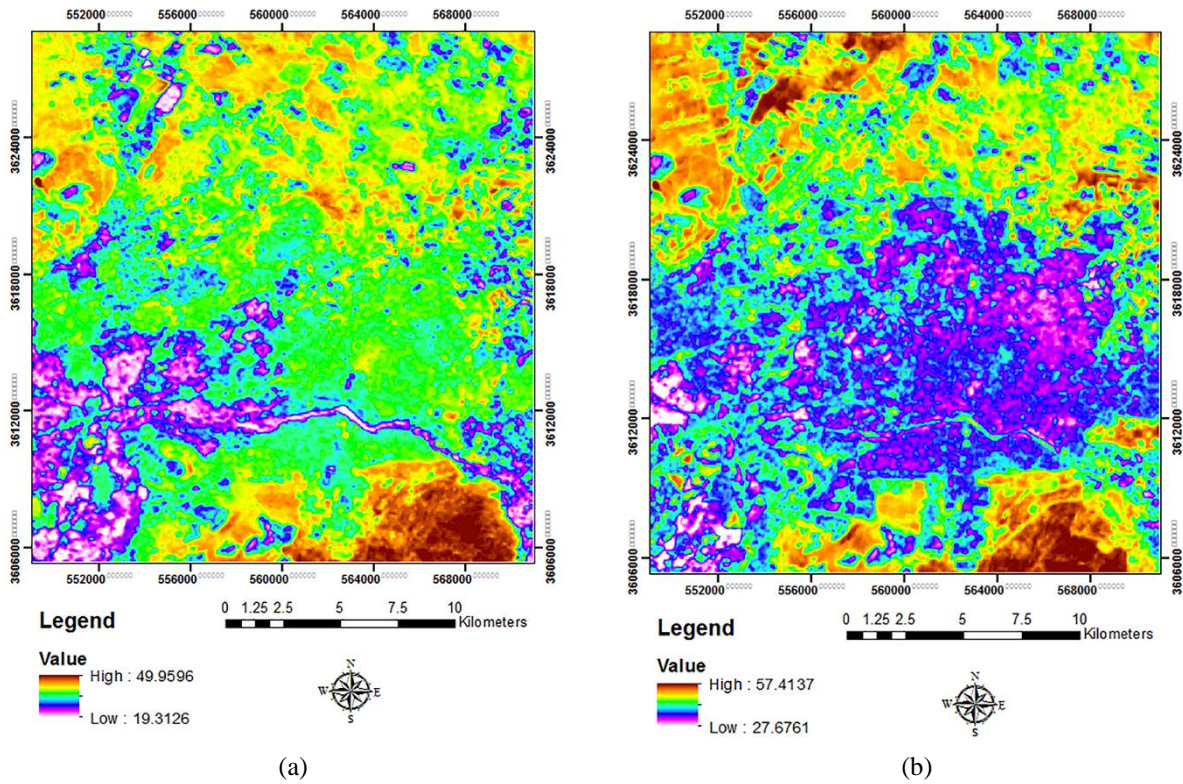


Figure 4. Land surface temperature layers for (a) 1998 and (b) 2014 node years

Table 5. Descriptive statistical parameters derived from resultant land surface temperature layers

Year	Minimum	Maximum	Mean	Std
1998	19.13	49.96	36.08	4.52
2014	27.68	57.41	43.86	4.78

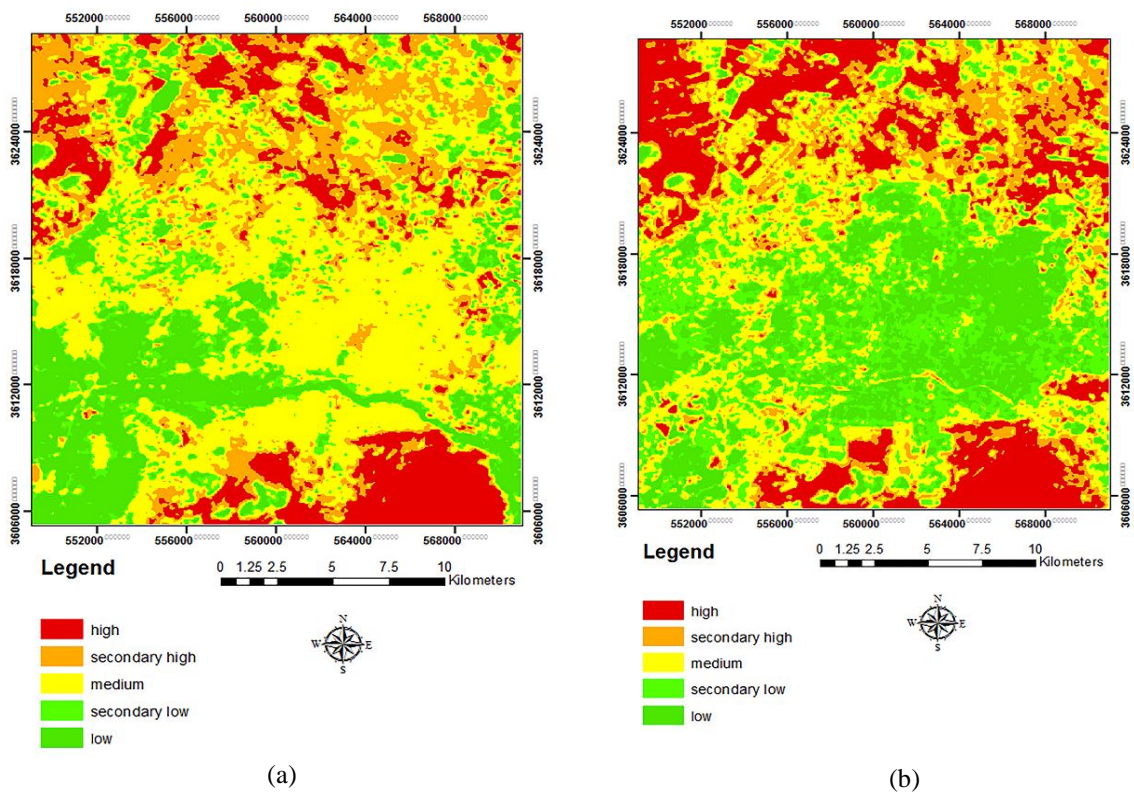


Figure 5. Classified land surface temperature layers for (a) 1998 and (b) 2014 node years

3.2 Analysing the dynamics of UHI in IMA

Table 6. Area of each land surface temperature category in 1998 and 2014 node years

LST classification	1998		2014	
	area (m <sup>2</sup> )	Proportion (%)	area (m <sup>2</sup> )	Proportion (%)
Low temperature area	78981718.69	15.49	87765677.35	17.21
Secondary low temperature area	48910639.2	9.59	105601840.6	20.71
Medium temperature area	226054570.2	44.33	145314242.4	28.50
Secondary high temperature area	88615492.77	17.38	69827970.25	13.69
High temperature area	67310079.14	13.20	101362769.4	19.9
Total	509872500	100	509872500	100

In order to evaluate changes in UHI from 1998 to 2014, a post-classification method was applied. The results of such

evaluation of changes in LST are shown in Figure 6 and Table 7.

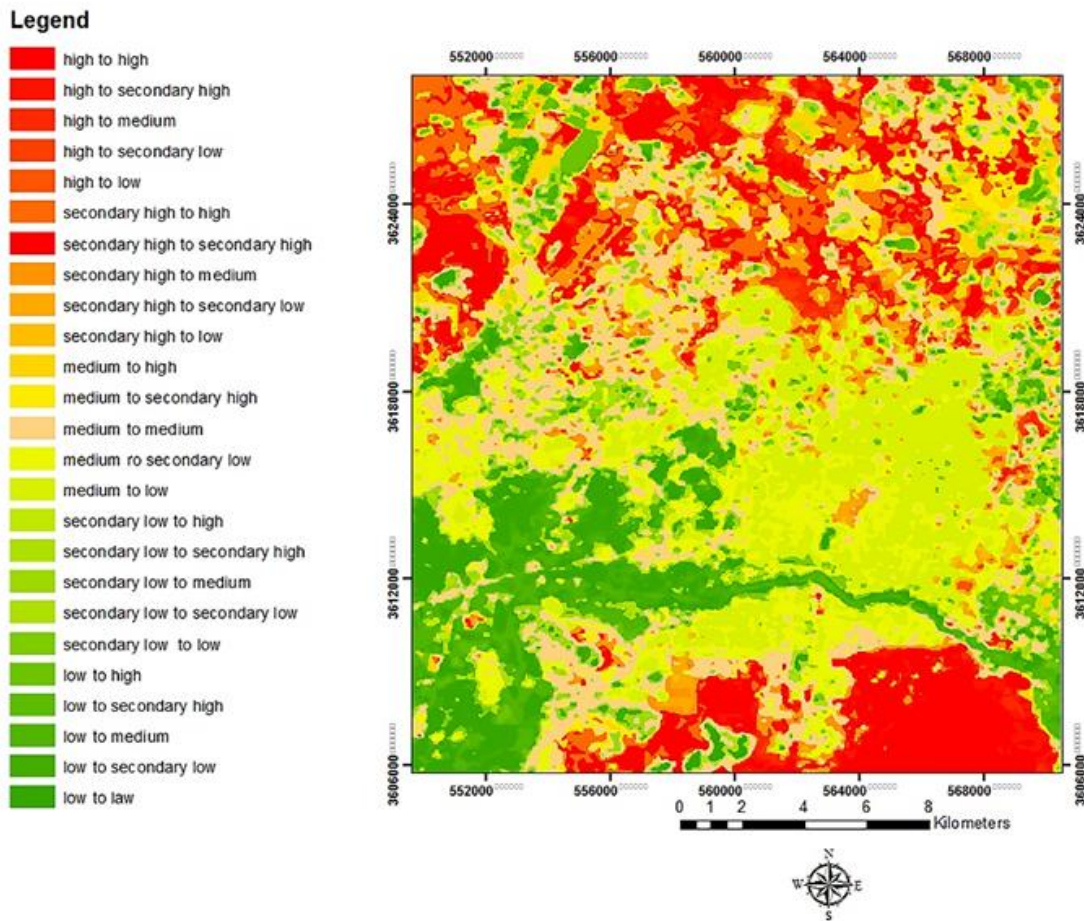


Figure 6. Cross-tabulated land surface temperature layers (1998-2014) and mutual exchanges between different temperature categories in Isfahan Metropolitan Area

Table 7. Mutual exchanges (%) between different land surface temperature categories during 1998-2014 time profile

		1998				
		High	Secondary high	Medium	Secondary low	Low
2014	High	72.189	32.517	6.834	8.021	5.765
	Secondary high	14.242	28.289	11.646	9.318	5.494
	Medium	9.763	25.888	31.707	42.063	29.498
	Secondary low	3.101	10.265	27.324	26.864	24.623
	Low	0.705	3.042	22.489	13.734	34.619

Besides, UHI effects can also be observed in eastern IMA, which is mainly due to the removal of green covers (Figure 3).

Based on figure 6, considerable changes in the UHI phenomenon appeared to be around the city center. In this regard, according to Table 7, LST values were decreased in 171.81 km<sup>2</sup> (36.53%) of the study area, while LST values increased over 150.20 km<sup>2</sup> (32%) of the study area. LST

values did not change for an area of 148.31 km<sup>2</sup>, which equals 31.53% of the total study area.

### 3.3 LST trend analysis

In this study, the Mann Kendall methodology was used to analyze the LST trend in IMA. Figure 7 provides an illustration of thermal environment dynamics in the study area.

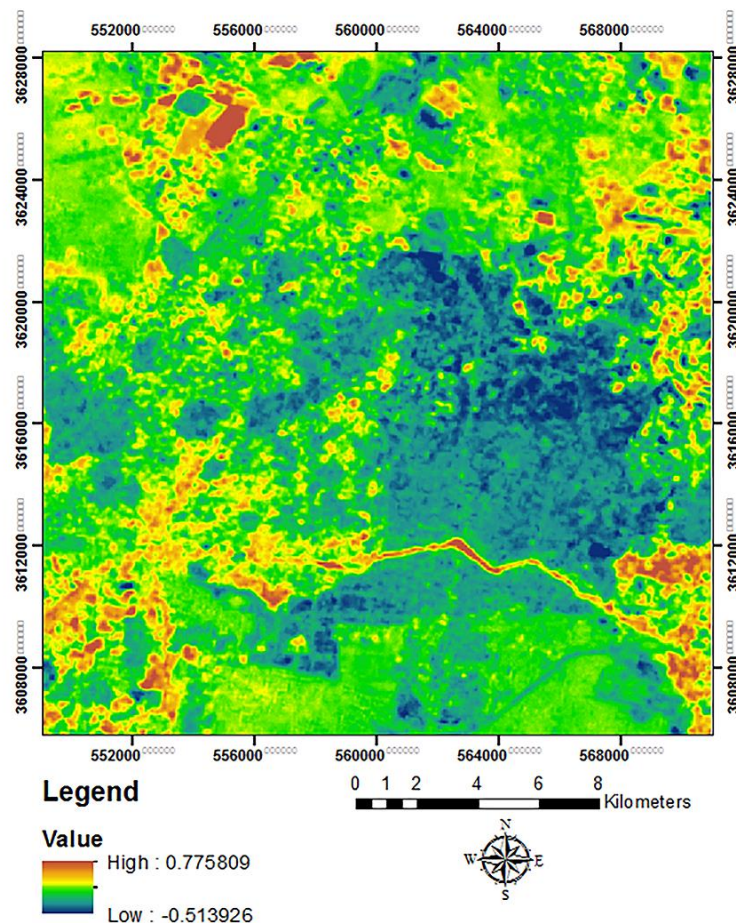


Figure 7. Pixel based Spatio temporal dynamics of land surface temperature in Isfahan Metropolitan Area during 1998-2014 time profile

Based on figure 7, areas with the biggest change in LST values are those near to 1, and areas with minimum change in LST values are those near to -1. Figure 6 demonstrates that surrounding areas compared to central locations have experienced an increasing LST trend and the intensity of this

trend is higher in the northwest and northeast of the research location. Furthermore, the margins of the Zayandeh-Rood seasonal river also observed drastic changes in LST. It represents the impact of the urban development and land-use changes on the spatial changes of UHI in IMA from 1998 to

2014.

In addition, Zayandeh-Rood seasonal river bed shows a drastic LST trend. The river in 2014 was dried up which indicates the river had a significant impact on the thermal environment of IMA. In this study in addition to analysis and evaluation of UHI Spatio-temporal dynamics, evaluation of UHI temporal change shows the URI index has increased from 0.25 in 1998 to 0.312 in 2014.

### 3.4 discussion

Analyzing the Spatio-temporal dynamics of the thermal environment in IMA provides valuable planning implications to inform the decision-makers for effective management in this region. Based on URI values distribution (Figure 7), the riverbank of Zayandeh-Rood and northwest and northeast of the study area have experienced a more drastic process of LST intensification, which can potentially lead to the formation of new UHI centers. In this regard, it should be mentioned that the Zayandeh-Rood riverine ecosystem has largely destructed due to the drying of the river during the study period. Although water flow is available through a very limited span across each year. Therefore, conservation of water bodies within interior urban environments and rehabilitation of Zayandeh-Rood River ecosystem can largely alleviate the thermal environment of the city and modifies the micro-climate in IMA. In this case, the construction of artificial water bodies near detected UHI hotspots can largely reduce the intensity of such phenomenon over the entire city. As regards the green covers demonstrate the low temperature. Using green covers in bare land or green roofs could be the best alternatives to reduce the LST rising trend in IMA (Bozorgi et al., 2018; Bozorgi & Nejadkoorki, 2019).

Referring to figures 6 and 7, newly constructed urban structures within urban boundaries have witnessed higher rates of LST increase. Simply, because urban boundaries are the locations that experienced a higher level of dynamics from low-temperature LST categories to high-temperature categories. This matter reflects the local characteristics of the study area. Specifically, due to factors such as available vacant lands and lack of effective regional regulations (Afrakhteh et al., 2016).

Cities in central Iran tend to expand their boundaries towards immediate vacant lands and agricultural fields, and therefore, cities experience a more compacted and connected pattern of urban growth in this region. Such a pattern of urban development leads to the construction of buildings in higher densities, and thus, these locations are the potential to form future UHI centers. In addition, urban growth is mainly associated with the consumption of green covers in central Iran (Asgarian et al., 2015), which can further exacerbate UHI formation conditions. Therefore, decentralized urban planning (Sakieh et al., 2015) could be considered as an available option for the conservation of green covers and

reduction of UHI effects. Based on decentralized urban planning, the construction of urban structures has occurred in more dispersed patterns; however, the spatial configuration of urban patches is regulated in terms of land suitability parameters for urban construction activities. In other words, a polycentric pattern of growth instead of high-density urban development is emphasized and urban vegetation covers under such pattern have a better chance to survive for encroachment of built structures. As indicated in previous studies (Sakieh et al., 2015; Afrakhteh et al., 2016; Sakieh et al., 2017), such pattern of urban growth allocation is associated with many ecological benefits such as lower LST values, calmer landscapes, and higher land potential for urban construction activities and biodiversity conservation (Goodarzi et al., 2017). In addition, Afrakhteh et al. (2016) highlight this strategy under the concept of smart rural development in central Iran. They argue that activation of rural growth cycles and minimization of growth rates in major urban centers can lead to the construction of a cooler landscape, in which both urban and rural environments are allowed to continue their growth profile under a controlled and planned situation. In addition, Afrakhteh et al. (2016) report that the physical size of the rural and small urban cores is the most powerful variable in describing the thermal environment in a city in central Iran. Therefore, area monitoring of newly constructed urban centers under the polycentric (or decentralized) planning strategy is recommended to prevent the formation and undesirable effects of the UHI phenomenon in central Iran.

### 4. Conclusion

Urban Heat Island is an important factor in urban ecosystems. This study analyzed and evaluated the changes of green covers and UHI in IMA, Iran for two decades. In former research, generally temporal changes of Land Surface Temperature (LST) were calculated, or just hot zones (Urban Heat Island) were identified. While in the current study, spatial changes of LST were determined. Moreover, temporal dynamics of the thermal environment in IMA were measured by Urban-Heat-Island Ration Index (URI). Results indicated that LST in IMA had an increasing trend over the period and the intensity of this trend was mainly concentrated in northwest and northeast of the city, destroyed green covers around Zayandeh-Rood River, and dried river bed. Temporal evaluation of UHI change indicated that the URI index had increased significantly. Results also demonstrated that the IMA not only witnessed an increase in the area of UHI but also the intensity of UHI has surged substantially between 1998 and 2014. In the period of research, a lot of green covers have turned to industrial and urban areas, Zayanderood River has dried and the green areas along which have been ruined. Although it is impossible to restore and change the urbanization development trend, we can manipulate managerial measures to alleviate the LST increasing trend in

IMA, Iran. All the analyses in this study were done employing remote sensing and the results indicated that satellite images were appropriate outfits for analyzing and evaluating green covers and UHI changes. Finally, using developed methods for LST retrieval (Jahani Mohammadi, 2014) is suggested, and also it is recommended that future research efforts study the causes of UHI dynamics especially in locations where there are higher densities of urban structures and higher intensities of anthropogenic activities.

## References

- Afrakhteh, R., Asgarian, A., Sakieh, Y. & Soffianian, A. (2016). "Evaluating the strategy of integrated urban-rural planning system and analyzing its effects on land surface temperature in a rapidly developing region." *Habitat International* 56: 147-156.
- Akbari, H., Pomerantz, M. & Taha, H. (2001). "Cool surfaces and shade trees to reduce energy use and improve air quality in urban areas." *Solar Energy* 70: 295-310.
- Amiri, R., Weng, Q., Alimohammadi, A. & Alavipana, SK. (2009). "Spatial-temporal dynamics of land surface temperature in relation to fractional vegetation cover and land use/cover in the Tabriz urban area, Iran." *Remote Sensing of Environment* 113(12): 2606-2617.
- Artis, DA. & Carnahan, WH. (1982). "Survey of emissivity variability in thermography of urban areas." *Remote Sensing of Environment* 12(4): 313-329.
- Asgarian, A., Amiri, B. J. & Sakieh, Y. (2015). "Assessing the effect of green cover spatial patterns on urban land surface temperature using landscape metrics approach." *Urban Ecosystems* 18(1): 209-222.
- Bozorgi, M. & Nejadkoorki, F. (2019). "Spatiotemporal monitoring of thermal environment in Isfahan Metropolitan Area" *SPRS International Geospatial Conference 2019* 4(W18): 227-234.
- Bozorgi, M., Nejadkoorki, F. & Mousavi, M.B. (2018). "Land surface temperature estimating in urbanized landscapes using artificial neural networks." *Environmental Monitoring and Assessment* 190(4): 1-10.
- Chakraborty, S. D., Kant, Y. & Mitra, D. (2013). "Assessment of land surface temperature and heat fluxes over Delhi using remote sensing data." *Journal of Environmental Management* 148: 143-152.
- Chen, A., Yao, X. A., Sun, R. & Chen, L. (2014). "Effect of urban green patterns on surface urban cool islands and its seasonal variations." *Urban Forestry and Urban Greening* 13(4): 646-654.
- Chen, Y., Chiu, H., Su, Y., Wu, Y. & Cheng, K. (2017). "Does urbanization increase diurnal land surface temperature variation? Evidence and implications." *Landscape and Urban Planning* 157: 247-258.
- Falahatkar, S., Soffianian, A. R., Khajeddin, S. J., Ziaee, H. R. & Ahmadi Nadoushan, M. (2011). "Integration of Remote Sensing Data and GIS for prediction of land cover map." *International Journal of Geomatics and Geosciences* 1: 847-864.
- Gobakis, K., Kolokotsa, D., Synnefa, A., Saliari, M., Giannopoulou, K. & Santamouris, M. (2011). "Development of a model for urban heat island prediction using neural network techniques." *Sustainable Cities and Society* 1: 104-115.
- Goodarzi, M. S., Sakieh, Y. & Navardi, S. (2017). "Measuring the effect of an ongoing urbanization process on conservation suitability index: integrating scenario-based urban growth modeling with conservation assessment and prioritization system (CAPS)." *Geocarto International* 32(8): 834-852.
- Guha, S. & Govil, H. (2020). "An assessment on the relationship between land surface temperature and normalized difference vegetation index." *Environment, Development, and Sustainability* 23: 1944-1963.
- Isfahan Meteorological Organization. (2014). Annual report of Isfahan Meteorology, Isfahan Meteorological Organization, Iran, <http://www.esfahanmet.ir/>.
- Islam, M.S. & Islam, K.S. (2013). "Application of thermal infrared remote sensing to explore the relationship between land use-land cover changes and Urban Heat Island effect: a case study of Khulna City." *Journal of Bangladesh Institute of Planners* 6: 49-60.
- Jahani, B. & Mohammadi, B. (2018). "A comparison between the application of empirical and ANN methods for estimation of daily global solar radiation in Iran." *Theoretical and Applied Climatology* 137: 1257-1269.
- Jing, J. & Guangjin, T. (2011). "Analysis of the impact of Land use/Land cover change on Land Surface Temperature with Remote Sensing." *International Society for Environmental Information Sciences 2010 Annual Conference (ISEIS)* 2: 571-575.
- Karimi, M., Shahedi, K. & Byzedi, M. (2015). "Analysis of Hydrological Drought using Constant Threshold Level Method (Case Study: Karkheh River Basin, Iran)." *Journal of Watershed Management Research* 6(11): 59-72.
- Kendall, MG. (1975). "Rank Correlation Methods", 4th edition, Charles Griffin, London. 410 p.
- Kumar, S., Merwade, V., Kam, J. & Thurner, K. (2009). "Streamflow trends in Indiana: Effects of long term persistence, precipitation and subsurface drains." *Journal of Hydrology* 374: 171-183.
- Mann HB. (1945). "Non-parametric tests against trend." *Econometrica* 13:163-171.
- Mirzaei, P. A. & Haghighat, F. (2010). "Approaches to study urban heat island—abilities and limitations." *Building and Environment* 45(10): 2192-2201.

- Oke, T. R. (1987). "Boundary layer climates." (London and New York: Methuen & Co)
- Oke, T. R. (1995). "The heat island of the urban boundary layer: Characteristics, causes, and effects." In J. E. Cermak (Ed.), *Wind climate in cities*. Netherlands: Kluwer Academic Publishers, 81-107.
- Rosenfeld, A. H., Akbari, H., Romn, J. J. & Pomerantz, M. (1998). "Cool communities: strategies for heat island mitigation and smog reduction." *Energy and Buildings* 28: 51–62.
- Rahimi, D. & Mohamadi, Z. (2017). "Assessing the hydrological drought of Zayande Rood Basin." *Geographical Planning of Space Quarterly Journal* 25: 221-233.
- Sakieh, Y., Jaafari, S., Ahmadi, M. & Danekar, A. (2017). "Green and calm: Modeling the relationships between noise pollution propagation and spatial patterns of urban structures and green covers." *Urban Forestry & Urban Greening* 24: 195-211.
- Sakieh, Y., Salmanmahiny, A., Jafarnezhad, J., Mehri, A., Kamyab, H. & Galdavi, S. (2015). "Evaluating the strategy of decentralized urban land-use planning in a developing region." *Land Use Policy* 48: 534–551.
- Schnur, MT., Hongjie, X. & Wang, X. (2010). "Estimating root zone soil moisture at distant sites using MODIS NDVI and EVI in a semi-arid region of southwestern USA." *Ecological Information* 5(5): 400–409.
- Singh, P., Kikon, N. & Verma, P. (2017). "Impact of land-use change and urbanization on urban heat island in Lucknow city, Central India. A remote sensing-based estimate." *Sustainable cities and society* 32: 100-114.
- Sobrino, JA., Oltra-Carrió, R., Sòria, G., JiménezMuñoz, JC., Franch, B., Hidalgo, V., Mattar, C., Julien, Y., Cuenca, J. & Romaguera, M. (2013). "Evaluation of the surface urban heat island effect in the city of Madrid by thermal remote sensing". *International Journal of Remote Sensing* 34 (9-10), 3177-3192.
- Songlin, C. & Tianxin, W. (2009). "Comparison Analyses of Equal Interval Method and Mean-standard Deviation Method Used to Delimitate Urban Heat Island". *Journal of Geoinformation Science* 11: 146–150.
- Taha, H., (1997). "Modeling the impacts of large-scale albedo changes on ozone air quality in the South Coast air basin". *Atmosphere Environment* 31: 1667–1676.
- Tayanç, M., Karaca, M. & Yenigün, O. (1997). "Annual and seasonal air temperature trends patterns of climate change and urbanization effects in relation with air pollutants in Turkey". *Journal of Geographical Research* 102(D2): 1909–1919.
- USGS. Landsat 7 (L7) Data Users Handbook. Available online: [https://prd-wret.s3-us-west-2.amazonaws.com/assets/palladium/production/atoms/files/LSDS1927\\_L7\\_Data\\_Users\\_Handbook-v2.pdf](https://prd-wret.s3-us-west-2.amazonaws.com/assets/palladium/production/atoms/files/LSDS1927_L7_Data_Users_Handbook-v2.pdf) (accessed on 5 December 2019).
- USGS. Landsat Normalized Difference Vegetation Index. [https://www.usgs.gov/core-science-systems/nli/landsat/landsat-normalized-difference-vegetation-index?qt-science\\_support\\_page\\_related\\_con=0#qt-science\\_support\\_page\\_related\\_con](https://www.usgs.gov/core-science-systems/nli/landsat/landsat-normalized-difference-vegetation-index?qt-science_support_page_related_con=0#qt-science_support_page_related_con)
- Voogt, J. A. & Oke, T. R. (2003). "Thermal remote sensing of urban climates." *Remote Sensing of Environment* 86: 370–384.
- Wu, J. G. (2014). "Urban ecology and sustainability: The state-of-the-science and future directions." *Landscape and Urban Planning* 125: 209–221.
- Xu, H. & Chen, B. (2004). "Remote sensing of the urban heat island and its changes in Xiamen City of SE China". *Journal of Environmental Sciences* 16: 411–418.
- Xunqiang, M., Cheng, C., Zhai, F. & Li, H. (2011). "Study on temporal and spatial variation of the urban heat island based on Landsat TM/ETM+ in central city and Binhai New Area of Tianjin." *2011 International Conference on Multimedia Technology* 4616-4622.
- Yang, Q., Huang, X. & Tang, Q. (2020). Irrigation cooling effect on land surface temperature across China based on satellite observations. *Science of The Total Environment* 705: 135984.
- Zhou, W., Huang, G. & Cadenasso, M. L. (2011). "Does spatial configuration matter? Understanding the effects of land cover pattern on land surface temperature in urban landscapes." *Landscape and Urban Planning* 102(1): 54–63.